



Published in final edited form as:

Biomed Microdevices. 2012 April ; 14(2): 357–366. doi:10.1007/s10544-011-9612-9.

Flexible microelectrode arrays to interface epicardial electrical signals with intracardial calcium transients in zebrafish hearts

Fei Yu,

Biomedical Engineering and Cardiovascular Medicine, University of Southern California, Los Angeles, CA, USA

Yu Zhao,

Electrical Engineering, California Institute of Technology, Pasadena, CA, USA

Jie Gu,

Biomedical Engineering and Cardiovascular Medicine, University of Southern California, Los Angeles, CA, USA

Katherine L. Quigley,

Biomedical Engineering and Cardiovascular Medicine, University of Southern California, Los Angeles, CA, USA

Neil C. Chi,

Department of Medicine, Division of Cardiology, University of California, San Diego, La Jolla, CA 92093-0613J, USA

Yu-Chong Tai, and

Electrical Engineering, California Institute of Technology, Pasadena, CA, USA

Tzung K. Hsiai

Biomedical Engineering and Cardiovascular Medicine, University of Southern California, Los Angeles, CA, USA. Cardiovascular Engineering Research Core, Biomedical Engineering and Cardiovascular Medicine, University of Southern California, Los Angeles, CA 90089, USA

Tzung K. Hsiai: hsiai@usc.edu

Abstract

The zebrafish (*Danio rerio*) is an emerging genetic model for regenerative medicine. In humans, myocardial infarction results in the irreversible loss of cardiomyocytes. However, zebrafish hearts fully regenerate after a 20% ventricular resection, without either scarring or arrhythmias. To study this cardiac regeneration, we developed implantable flexible multi-microelectrode membrane arrays that measure the epicardial electrocardiogram signals of zebrafish in real-time. The microelectrode electrical signals allowed for a high level of both temporal and spatial resolution (~20 μm), and the signal to noise ratio of the epicardial ECG was comparable to that of surface electrode ECG (7.1 dB vs. 7.4 dB, respectively). Processing and analysis of the signals from the microelectrode array demonstrated distinct ECG signals: namely, atrial conduction (P waves), ventricular contraction (QRS), and ventricular repolarization (QT interval). The electrical signals were in synchrony with optically measured Calcium concentration gradients in terms of $d[\text{Ca}^{2+}]/dt$ at both whole heart and tissue levels. These microelectrodes therefore provide a real-time analytical tool for monitoring conduction phenotypes of small vertebral animals with a high temporal and spatial resolution.

Keywords

Zebrafish hearts; Flexible electronics; ECG; Cardiac conduction; Calcium waves

1 Introduction

Real-time monitoring of heart regeneration in a vertebrate model system is highly relevant to tissue engineering and stem cell therapy. Myocardial infarction results in irreversible loss of cardiac tissue (Reeve et al. 2005). Injured human hearts heal by scarring, which leads to remodeling, arrhythmia, and heart failure (Hahn and Schwartz 2008). In contrast, Zebrafish (*Danio rerio*) fully regenerate their myocardium after 20% ventricular amputation (Poss et al. 2002; Raya et al. 2004), thus providing a genetically tractable model system for high-throughput research, including antiarrhythmic (Zon and Peterson 2005) and psychoactive drug discoveries (Rihel et al. 2010; Mitcheson et al. 2000), as well as human inherited cardiac arrhythmias, blood, and sleep disorders (Stoletov et al. 2009; Yokogawa et al. 2007).

Zebrafish hearts harbor remarkably similar cardiac electrical properties as those of humans (Sedmera et al. 2003). In addition to their similar surface electrical cardiograms (ECG) (Fig. 7(a)) (Milan and MacRae 2005), the critical pathways in cardiovascular development parallel to higher vertebrates (Stainier 2001). Histological studies show that the ventricle of adult zebrafish hearts is composed of trabecular myocardium and compact myocardium, surrounded by epicardium and endocardium. More importantly, genes involved in zebrafish heart development are highly conserved with higher vertebrates. In terms of size, the average length of an adult fish is at 2 to 4 cm. The mean heart rate is at 151 ± 30 beats/min, and the pericardial sac is encased in the thoracic cavity below the pectoral fin at 1 mm beneath the skin. While the small size is conducive to high-throughput research, the small heart size (1–2 mm in length) renders it challenging to perform functional physiological analyses. In this context, the advent of flexible micro-electronics allows for interrogation of small animal systems in real-time.

Here, we demonstrated electrical and optical coupling of cardiac conduction in zebrafish hearts via flexible microelectrodes with high spatial resolution otherwise difficult with the existing external needle electrodes (Forouhar et al. 2004; Milan and MacRae 2005; Sun et al. 2009). We implanted one counter and three detecting microelectrodes to the chest cavity of adult zebrafish and the reference electrodes to the tails. Application of signal processing and wavelet transform revealed three distinct epicardial ECG recordings at 10 μm apart. In corollary, we demonstrated that intracellular Calcium transients (Ca^{2+}) in the single cell and tissue levels were in synchrony with the epicardial ECG recordings. Thus, interfacing flexible microelectrodes provides enhanced spatial resolution at $\sim 5 \mu\text{m}$ for real-time longitudinal monitoring of electrical signals from the non-planar and dynamic cardiac surface.

2 Methods

2.1 Animals

The animal experiments were performed in compliance with the protocol approved by the Institutional Animal Care and Use Committee (IACUC) at the University of Southern California. Adult zebrafish, 3–5 cm in length, were acquired from Tong's Tropical Fish and Supplies (CA) and maintained under standard laboratory conditions at 24°C. The individual fish were fed daily with brine shrimp (hatched from eggs in 10 ml in 2 L salt water), and were kept in constantly circulating water.

2.2 Microfabrication of flexible electrode arrays

Approximately 10 μm of parylene C was deposited on a silicon wafer with a photoresist sacrificial layer to the underside (Fig. 1). A second layer of photoresist was deposited, followed by selective exposure and development to a diamond-shape pattern. Next, a gold layer was deposited via Physical Vapor Deposition (PVD) via a titanium adhesion layer. Gold metal liftoff process was used to define pitches with a thickness from 200 nm to 300 nm. A final parylene coating at approximately 2 μm in thickness formed the top insulation layer. The electrodes and connection pads were exposed and the overall geometry of the array was defined by oxygen plasma reactive-ion etching via a thick photoresist etch mask. Finally, the arrays were peeled from the wafer in a water bath or released through removal of the sacrificial photoresist in acetone (Fig. 2(a)).

2.3 Microelectrode array implantation

The fish were sedated using tricaine methanesulfonate (MS-222), and placed in a damp sponge to expose the ventral side for visualization under the microscope as previously described (Sun et al. 2009; Yu et al. 2010). Two parallel incisions of approximately 1.5 mm in length and 1.5 mm apart were performed on the chest (Fig. 2(b)), and two triangular structures of the chest stripe were inserted into the incision sites for direct microelectrode contact with the epicardium. The tail stripe was placed on the abdominal region with the reference electrode in contact with the abdominal skin. Both parylene-coated stripes were sutured to the fish body.

2.4 Data processing of epicardial ECG signals

The ECG measurements were performed using a modified technique (Sun et al. 2009). The entire recording processes were performed in a Faraday cage to shield interference from electromagnetic radiation. The ECG signals were amplified by 10,000-fold (A-M Systems Inc. 1700 Differential Amplifier, Carlsborg, WA), and were filtered at a cutoff frequency of 60 Hz (notch) between 0.1 and 500 Hz. The signals were acquired and digitized at a sampling rate of 1,000 Hz (National Instruments USB-6216 DAQ device, Austin TX, and LabVIEW 8.2). Wavelet transform and thresholding analysis were applied to enhance signal-to-noise ratios (Matlab 2007a software, MathWorks, Inc.) for the individual ECG signals recording as previously reported (Sun et al. 2009).

Wavelet transform was performed to filter various sources of noise. A wavelet was a mathematical function used to divide a given function or continuous-time signal into different frequency components. The individual components were investigated with a resolution corresponding to their scales. Wavelet transform represented a function by scaled wavelets in time domain (Szilagyí and Szilagyí 2000). After ECG signals were digitized at a rate of 1,000 Hz, the digital signals were divided into 10 scales by using “coif5” wavelet. The coif5 is a 5th order coiflet (a discrete wavelet) function designed (by Ingrid Daubechies) (Burrus et al. 1997) to enable the best performance for de-noising ECG signals (Tan et al. 2007). Wavelet transform further allowed for a high speed convergence to reduce computation time (Donoho 1995). Thresholding analysis was applied to suppress the gill motion noise that was merged within ECG signals. The remaining signals were recomposed by the inverse wavelet transform, resulting in the de-noised ECG signals. P wave (atrial contraction), QRS complexes (ventricular contraction) and ST segment (ventricular repolarization) were distinguishable for the epicardial ECG recordings, and QRS intervals were measured from the beginning of upstroke (Q) to the troughs (S). The signal-to-noise ratio (SNR) in decibel was calculated before and after processing using the following formula:

$$\text{SNR} = 20 \log_{10} \frac{A_{\text{signal}}}{A_{\text{noise}}} \quad (1)$$

Where A is the root mean square (RMS) voltage for signal and noise, respectively. SNR for the epicardial ECG recordings and surface ECG recordings were compared to evaluate the feasibility of electrode array-based epicardial ECG applications.

2.5 Optical calcium transients in the entire and apical region of the adult zebrafish hearts

Intracellular cardiomyocyte calcium concentrations allowed for monitoring the propagation of electrical signal across the heart with a 320×240 pixels resolution. The experimental setup and methods for simultaneous optical imaging of Calcium were described previously (Valderrabano et al. 2006). In brief, adult zebrafish were sedated in a 0.02% solution of Tricaine Methanesulfonate in water until they stop moving completely. Hearts were removed from the fish via midline incision and were then incubated in incubation solution (IS) containing 5 μM Fluo-4-acetoxymethyl ester dissolved in dimethyl sulfoxide and pluronic F-127 (0.1%) (Invitrogen) for 40 min. Hearts were then washed in Tyrode's solution (in mM, NaCl 136, KCl 5.4, NaH₂PO₄ 0.3, MgCl₂ 1.0, Glucose 5.0, HEPES 10 and CaCl₂ 1.8, pH adjusted to 7.4 with NaOH) before transferring to an experimental chamber ($T=23^{\circ}\text{C}$) on a inverted microscope (Olympus). Whole heart Calcium imaging was performed with a resolution of 320×240 pixels at 30 frames/second using a CCD camera (Model LCL 811K, Watec America, Las Vegas, NV)(Chen et al. 2006) and apical heart imaging was recorded by a digital camera (Canon EOS 550D) at 50 frames per second. Optical mapping and myocardial calcium dynamics were superimposed to provide direct comparison.

2.6 Optical calcium transients in a single cell

After heart was removed from fish as described above, ventricle was isolated under microscope. Ventricles then will be digested in the calcium-free salt solution (SS) containing the following (in mM): NaCl 136, KCl 5.4, NaH₂PO₄ 0.33, HEPES 10 (pH 7.4) supplemented with 0.1 mg/mL trypsin and 1 mg/mL collagenase. Digestion was allowed at 37°C for 20 min. The tissue was then transferred into SS supplemented with 0.1 mM CaCl₂ and 1 mg/mL BSA, and cells were isolated by gentle trituration using fire-polished pasteur pipette of different pore sizes.

Next, isolated cardiomyocytes were centrifuged and resuspended with the IS for 30mins. After incubation cells were washed and transferred into standard Tyrode's solution for imaging. ImageJ (NIH) and Matlab (Mathworks) software were used for data processing.

3 Results

3.1 Epicardial ECG signal processing

The initial ECG signals were recorded at 1,000 Hz (Fig. 3(a)). Wavelet transform was performed by breaking down the signals into 10 frequency segments ranging from 0 Hz to the Nyquist frequency (½ of sampling frequency, i.e. 500 Hz) (Fig. 3(b)) (Sun et al. 2009). The individual frequency ranges contained different levels of signal components in the presence of noise, which was suppressed by the pre-set threshold value (Fig. 3(b)). Signals in the frequency range between 0.98 Hz and 7.8 Hz were not filtered to preserve T wave (Sun et al. 2009). The final ECG signals were re-constructed by inverse wavelet transform after noise reduction (Fig. 3(c)). The P waves, QRS complexes and T waves were retained,

allowing for significantly improved signal-to-noise ratios from approximately 2 dB for the raw data to 7 dB after processing.

3.2 Epicardial ECG versus surface ECG signals

Implantation of flexible microelectrode arrays in the zebrafish myocardium revealed distinct P waves, QRS complexes and T waves (Fig. 4). While ECG signals recorded from Electrodes A and B revealed high amplitude QRS complexes (Fig. 4(a) and (b)), electrode C revealed low amplitude QRS complexes and inverted ST segments (Fig. 4(c)). In comparison with the surface ECG signals (Fig. 4(d)), epicardial microelectrode array demonstrated a higher signal strength (1.1 V) compared to surface needle microelectrodes (0.8 V) with comparable SNR (7.1 dB vs. 7.4 dB for epicardial ECG and surface ECG, respectively).

3.3 Interfacing epicardial ECG signals with propagation of calcium transient in the entire hearts

Excitation conduction across the myocardium revealed propagation of electrical signals beginning from the atrium (A), through AV ring (AVR), to the ventricle (V) (Fig. 5). In response to cardiac contraction, a sequence of intracellular Calcium transients was captured in an area measured at $1870 \times 1400 \mu\text{m}^2$, accompanied by an image resolution of 320×240 pixels. As the Calcium transients propagated from the atrium, through the AV ring, to the ventricle (Fig. 5(b)), instantaneous changes in Ca^{2+} as a function of time were consistent with the sequence of atrial contraction (P waves) and ventricular contraction (QRS complexes). Isochronal map revealed that fast conduction rate developed in both atrium and ventricle as evidenced by the longer distance between the white dash lines, whereas slow conduction rate occurred in the AV ring region as evidenced by a shorter distance between the dash lines (Fig. 5(c)). The sequence of pseudo-colored snapshots of Ca^{2+} fluorescence corresponded to atrial contraction from 0 ms to 167 ms (P waves); ventricular contraction was initiated within the first 167 ms (QRS complexes) and propagated up to 267 ms, followed by ventricular repolarization until 400 ms (ST segments) (Fig. 5(d)). Thus, application of Calcium mapping provided a basis to validate conduction phenotypes from epicardial ECG signals.

3.4 Interfacing epicardial ECG signals with intracardiac calcium transients in a single cell and an apical region

In corollary, Calcium transients were captured in the apical region of a contracting ventricle (Fig. 6(a)). The mean grey value intensity plots of the five regions of interests (ROIs) revealed Calcium transients, $d[\text{Ca}^{2+}]/dt$, in synchrony with the epicardial ECG signals (Fig. 6(b)). Intracellular Calcium transients were also captured in three ROIs from a single contracting cardiomyocyte (Fig. 6(c)). Corresponding mean fluorescence intensity plots demonstrated propagation of Calcium transients at single cell level (Fig. 6(d)). Thus, epicardial ECG recordings provide a reliable means of label-free monitoring of conduction phenotypes.

4 Discussion

Heart failure inflicts nearly 5 million people in the US, and an additional 550,000 new cases are diagnosed each year. Despite current regimens, heart failure remains the leading cause of morbidity and mortality in the United States and developed world mainly from inadequate replacement of infarcted myocardium. Despite limited capacity for cardio-myocytes to divide, this regeneration is insufficient to overcome the significant loss of myocardium (Hsieh et al. 2007; Bergmann et al. 2009; Bersell et al. 2009). However, zebrafish (*Danio rerio*) possess a remarkable capacity to regenerate a significant amount of myocardium in

injured hearts, and thus, represent a viable vertebrate model for regeneration (Poss et al. 2002).

In this study, we demonstrated real-time recordings of electrical conduction phenotypes in small vertebral animal such as zebrafish via flexible microelectrode arrays. Distinct P waves, QRS complexes, and ST segments were comparable to those of surface ECG. Furthermore, the dynamic intracellular Calcium transients were in synchrony with the epicardial ECG signals, and propagation of Calcium from the atrium to ventricle was coupled with one cycle of ECG signals. Thus, interfacing flexible microelectrodes with the epicardium was conducive to real-time recording of electrical signals from the contracting hearts with high spatial resolution at $\sim 20 \mu\text{m}$.

The advent of flexible microelectrodes allows for physiological interrogation of the small animal systems at the interface between electronics and living tissue (Yu et al. 2008; Rodger et al. 2006B). Flexible intravascular thermal sensors have been deployed to the aortas of New Zealand White rabbits model on hypercholesterolemic diet to assess arterial regions prone to atherosclerotic plaques (Yu et al. 2011). Novel flexible parylene-based high-density electrode arrays have also been applied for electrical stimulation in the retinas and spinal cords (Rodger et al. 2007). These electrode arrays were micro-fabricated according to single-metal-layer and, most recently, by the dual-metal-layer processes. Electrode arrays have also been implanted and tested in the spinal cords of murine models, with the ultimate goal of restoring locomotion post spinal cord injury. These arrays provide a high density and precise spatial control of stimulation and recording otherwise impossible with the traditional fine-wire electrodes (Rodger et al. 2006a). Furthermore, with the recent advancement of epidermal electronic technologies (Kim et al. 2011), long-term epicardial ECG monitoring for small vertebrates in aqueous environment are made possible with wireless powered, implantable multielectrode microelectronics.

Dipole, the polarity of the cardiac pacemaker, the distance of the electrode from the dipole, and the strength of the electrical field influence ECG recording (Braunwald et al. 2004). For example, the amplitude of ventricular contraction (QRS) signals varies depending on the distance and direction from the dipole (Fig. 7). The strength of electric potential (E_p) is proportional to the solid angle (Ω) and charge surface ($\Phi = \text{voltage/unit of the solid angle}$), and is inversely proportional to the square of the distance from the source. Consistent with the 12-lead surface ECG signals in humans, the amplitude and shape of QRS complexes and ST segments varied depending on the solid angle (Ω) and the strength of charge surface ($\Phi = \text{voltage/unit of the solid angle}$) from the pacemaker source or dipole (Fig. 4). Compared to previously reported surface ECG recording (Fei Yu et al. 2010), the epicardial multielectrode ECG system was able to provide information about the pacemaker dipole as well as the asymmetry of the ventricle repolarization, and will be particularly useful in monitoring ECG changes during heart regeneration.

In this study, we also demonstrated that epicardial ECG signals correlated with optical Calcium transients in the whole hearts. Optical Calcium transients required resection of the entire hearts or isolation of cardiomyocytes from the fish, whereas epicardial ECG recordings were performed in real-time without sacrificing the animals. While Calcium transients revealed contraction of individual cardiomyocyte and atrioventricular activation in the entire hearts, flexible microelectrodes allow for a global assessment of electric conduction from atrial contraction to ventricular contraction and repolarization. In addition, Calcium dye is cytotoxic, undergoing photobleaching during prolonged recording. Thus, interfacing flexible microelectrodes with contracting epicardium offered a non-invasive and long-term strategy to assess tissue regeneration.

Overall, flexible microelectrodes provided an entry point to identify the specific electrical responses to tissue injury, drug-screening, and regenerating hearts. These phenotypic effects are otherwise difficult with optical mapping alone. By allowing for direct electrode contact with the non-planar surface of the pericardium, epicardial ECG signals will further address the inter-observer and inter-lab variations, as well as changes in solid angles between trials with the use of a pair of microelectrodes. Furthermore, application of flexible microelectrodes allows for addressing a higher pacing threshold in the regenerating part of the heart where the regenerated myocardium is not fully conductive. In the era of regenerative medicine, flexible microelectrodes are conducive to maintain a connection with the living tissues without damaging the host cells; thus, enabling longitudinal monitoring of the conduction phenotypes in the specific regions of injured and regenerating myocardium.

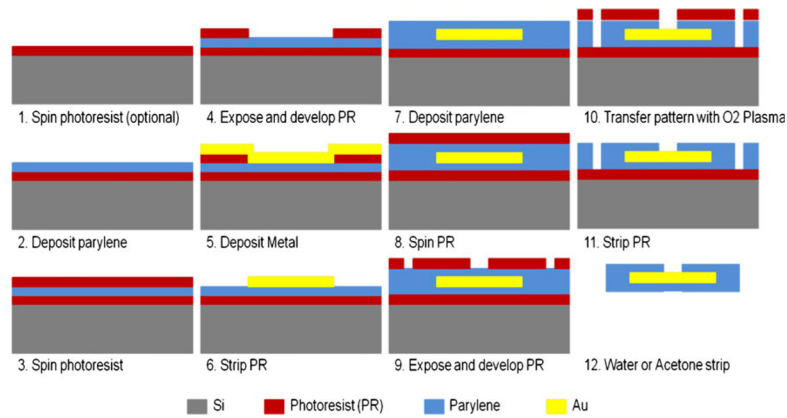
Acknowledgments

The authors would like to express gratitude for Dr. Fuhua Chen from UCLA School of Medicine for providing the Calcium voltage mapping. This project was supported by the American Heart Association Pre-Doctoral Fellowship (11PRE7370088) (FY), National Institutes of Health, National Heart Lung and Blood Institute (HL083015) (TKH), HL091302 (TKH), (HL104239) (NCC) and National Institute of Child Health & Human Development (HD069305) (NCC and TKH).

References

- Bergmann O, Bhardwaj RD, Bernard S, Zdunek S, Barnabe-Heider F, Walsh S, et al. Evidence for cardiomyocyte renewal in humans. *Science*. 2009; 324(5923):98.10.1126/science.1164680 [PubMed: 19342590]
- Bersell K, Arab S, Haring B, Kuhn B. Neuregulin1/ErbB4 signaling induces cardiomyocyte proliferation and repair of heart injury. *Cell*. 2009; 138(2):257.10.1016/j.cell.2009.04.060 [PubMed: 19632177]
- Braunwald, E.; Zipes, DP.; Libby, P.; Bonow, R., editors. Braunwald's heart disease: a textbook of cardiovascular medicine. 7. Saunders Company; Philadelphia: 2004.
- Burrus, CS.; Gopinath, RA.; Guo, H. Introduction to wavelets and wavelet transforms: a primer. Prentice-Hall; Upper Saddle River: 1997.
- Chen F, Klitzner TS, Weiss JN. Autonomic regulation of calcium cycling in developing embryonic mouse hearts. *Cell Calcium*. 2006; 39(5):375.10.1016/j.ceca.2005.12.004 [PubMed: 16545869]
- Donoho DL. De-noising by soft-thresholding. *IEEE Trans Inform Theor*. 1995; 41(3):613.
- Forouhar AS, Hove JR, Calvert C, Flores J, Jadvar H, Gharib M. Electrocardiographic characterization of embryonic zebrafish. *Conf Proc IEEE Eng Med Biol Soc*. 2004; 5:3615. [PubMed: 17271074]
- Hahn C, Schwartz MA. The role of cellular adaptation to mechanical forces in atherosclerosis. *Arterioscler Thromb Vasc Biol*. 2008; 28(12):2101. [PubMed: 18787190]
- Hsieh PC, Segers VF, Davis ME, MacGillivray C, Gannon J, Molkenin JD, et al. Evidence from a genetic fate-mapping study that stem cells refresh adult mammalian cardiomyocytes after injury. *Nat Med*. 2007; 13(8):970.10.1038/nm1618 [PubMed: 17660827]
- Kim DH, Lu N, Ma R, Kim YS, Kim RH, Wang S, et al. Epidermal electronics. *Science*. 2011; 333(6044):838. [PubMed: 21836009]
- Milan DJ, MacRae CA. Animal models for arrhythmias. *Cardiovasc Res*. 2005; 67(3):426. [PubMed: 16009355]
- Mitcheson JS, Chen J, Lin M, Culberson C, Sanguinetti MC. A structural basis for drug-induced long QT syndrome. *Proc Natl Acad Sci U S A*. 2000; 97(22):12329. [PubMed: 11005845]
- Poss KD, Wilson LG, Keating MT. Heart regeneration in zebrafish. *Science*. 2002; 298(5601):2188. [PubMed: 12481136]
- Raya A, Consiglio A, Kawakami Y, Rodriguez-Esteban C, Izpisua-Belmonte JC. The zebrafish as a model of heart regeneration. *Clon Stem Cell*. 2004; 6(4):345.
- Reeve JL, Duffy AM, O'Brien T, Samali A. Don't lose heart—therapeutic value of apoptosis prevention in the treatment of cardiovascular disease. *J Cell Mol Med*. 2005; 9(3):609. [PubMed: 16202209]

- Rihel J, Prober DA, Arvanites A, Lam K, Zimmerman S, Jang S, et al. Zebrafish behavioral profiling links drugs to biological targets and rest/wake regulation. *Science*. 2010; 327(5963):348. [PubMed: 20075256]
- Rodger DC, Weiland JD, Humayun MS, Tai YC. Scalable high lead-count parylene package for retinal prostheses. *Sensor Actuator B Chem*. 2006a; 117(1):107.
- Rodger, DC.; Li, W.; Fong, H.; Ameri, AJ.; Meng, E.; Burdick, J., et al. Flexible microfabricated parylene multielectrode arrays for retinal stimulation and spinal cord field modulation. *Proc. 4th International IEEE-EMBS Special Topic Conference on Microtechnologies in Medicine and Biology ((MMB'06); Okinawa, Japan. 2006b. p. 31*
- Rodger, DC.; Fong, AJ.; Li, W.; Ameri, H.; Lavrov, I.; Zhong, H., et al. High-density Flexible Parylene-based Multielectrode Arrays for Retinal and Spinal Cord Stimulation. *Transducers '07; Lyon: 2007.*
- Sedmera D, Reckova M, deAlmeida A, Sedmerova M, Biermann M, Volejnik J, et al. Functional and morphological evidence for a ventricular conduction system in zebrafish and *Xenopus* hearts. *Am J Physiol Heart Circ Physiol*. 2003; 284(4):H1152. [PubMed: 12626327]
- Stainier DY. Zebrafish genetics and vertebrate heart formation. *Nat Rev Genet*. 2001; 2(1):39. [PubMed: 11253067]
- Stoletov K, Fang L, Choi SH, Hartvigsen K, Hansen LF, Hall C, et al. Vascular lipid accumulation, lipoprotein oxidation, and macrophage lipid uptake in hypercholesterolemic zebrafish. *Circ Res*. 2009; 104(8):952. [PubMed: 19265037]
- Sun P, Zhang Y, Yu F, Parks E, Lyman A, Wu Q, et al. Micro-electrocardiograms to study post-ventricular amputation of zebrafish heart. *Ann Biomed Eng*. 2009; 37(5):890. [PubMed: 19280341]
- Szilagyi, SM.; Szilagyi, L. Wavelet transform and neural-network-based adaptive filtering for QRS detection. *Proceedings: 22nd Annual IEEE - EMBS International Conference; 2000. p. 1267*
- Tan, HGR.; Tan, A.; Khong, P.; Mok, V. Best wavelet function identification system for ecg signal denoise applications. *Proceedings of International Conference on Intelligent and Advanced Systems; International Conference on Intelligent and Advanced Systems; Kuala Lumpur. 2007; IEEE; 2007. p. 631*
- Valderrabano M, Chen F, Dave AS, Lamp ST, Klitzner TS, Weiss JN. Atrioventricular ring reentry in embryonic mouse hearts. *Circulation*. 2006; 114(6):543.10.1161/CIRCULATIONAHA.106.633727 [PubMed: 16880324]
- Yokogawa T, Marin W, Faraco J, Pézerson G, Appelbaum L, Zhang J, et al. Characterization of Sleep in Zebrafish and Insomnia in Hypocretin Receptor Mutants. *PloS Biol*. 2007; 5(10):2379.
- Yu H, Ai L, Rouhanizadeh M, Patel D, Kim ES, Hsiai TK. Flexible polymer sensors for *in vivo* intravascular shear stress analysis. *J Microelectromech Syst*. 2008; 17(5):1178.
- Yu F, Li R, Parks E, Takabe W, Hsiai TK. Electrocardiogram signals to assess zebrafish heart regeneration: implication of long QT intervals. *Ann Biomed Eng*. 2010; 38(7):2346. [PubMed: 20221900]
- Yu F, Ai L, Dai W, Yu H, Hsiai TK. MEMS thermal sensors to detect changes in heat transfer in the pre-atherosclerotic regions of fat-fed New Zealand white rabbits. *Ann Biomed Eng*. 2011; 39(6):1736. [PubMed: 21380571]
- Zon LI, Peterson RT. *In vivo* drug discovery in the zebrafish. *Nat Rev Drug Discov*. 2005; 4(1):35. [PubMed: 15688071]

**Fig. 1.**

Microfabrication steps for flexible microelectrode arrays. The microelectrode array is embedded in a sandwich structure as parylene-metal-parylene. **Steps 1–4:** Approximately 8 μm of parylene C was deposited on a silicon wafer, followed by spin-coating with a photoresist sacrificial layer. **Steps 5–6:** A gold metal liftoff process was used to define a 16 μm pitch with a thickness from 200 nm to 300 nm. **Step 7:** A second parylene deposition ($\sim 1 \mu\text{m}$) formed the insulation. **Steps 8–10:** A small via at 6 $\mu\text{m} \times 6 \mu\text{m}$ was patterned in the insulation layer by oxygen plasma reactive-ion etching. **Step 11:** The top layer of photoresist was striped to expose the microelectrode arrays. **Step 12:** The arrays were peeled from the wafer in a water bath or released through removal of the sacrificial photoresist in acetone

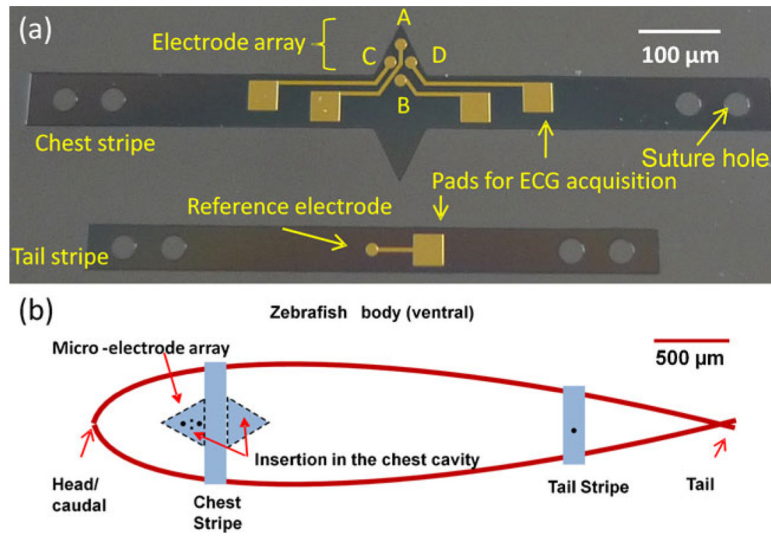


Fig. 2. (a) Flexible microelectrode arrays for zebrafish ECG recording. The chest strip (upper electrodes) consisted of detecting electrodes (A, C, and D) and the tail strip (lower electrode) consisted of a reference electrode. (b) Microelectrode array implantation scheme. The chest strip was inserted into the chest cavity above the pericardium. The tail strip was secured to the tail

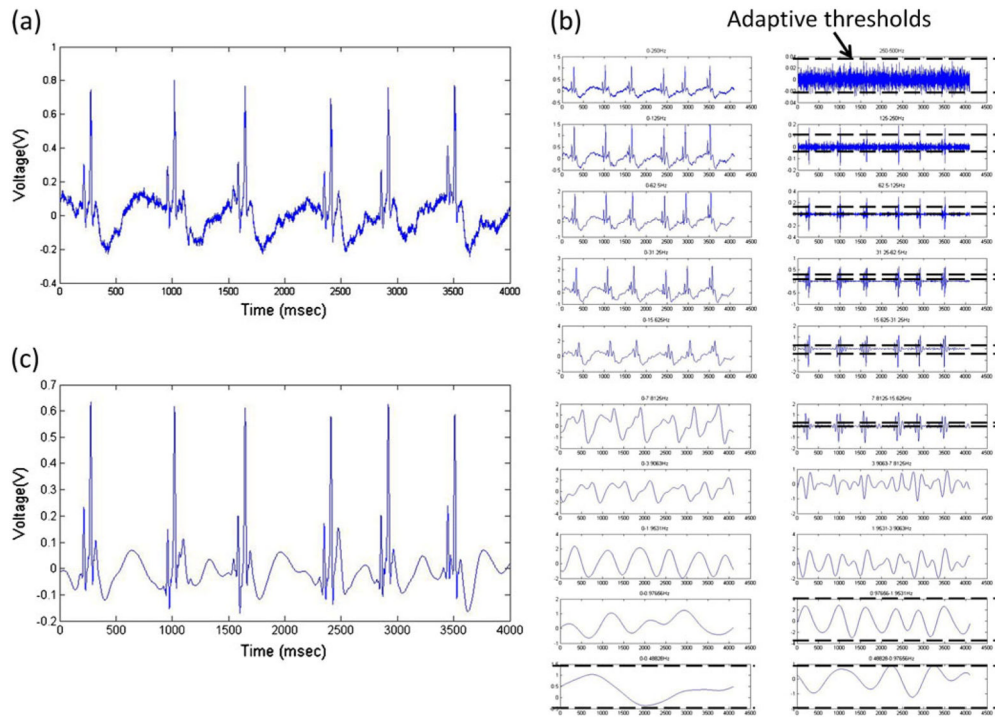


Fig. 3. Wavelet transform and noise-reduction algorithm for zebrafish ECG recordings. **(a)** Raw signal directly recorded from sedated zebrafish at sampling rate of 1000 Hz. **(b)** Breakdown of raw signals into frequency segments via *coif5* wavelet transform. Low frequency signals (DC to 0.98 Hz) were completely filtered. Thresholds were applied to the individual frequency ranges for suppression of corresponding noise levels. Sub-threshold values were set to zero. Signals within frequency range from 0.98 Hz to 7.81 Hz were reserved to ensure fidelity of T-waves. **(c)** Filtered ECG signals were reconstructed by performing inverse wavelet transform from processed frequency segments

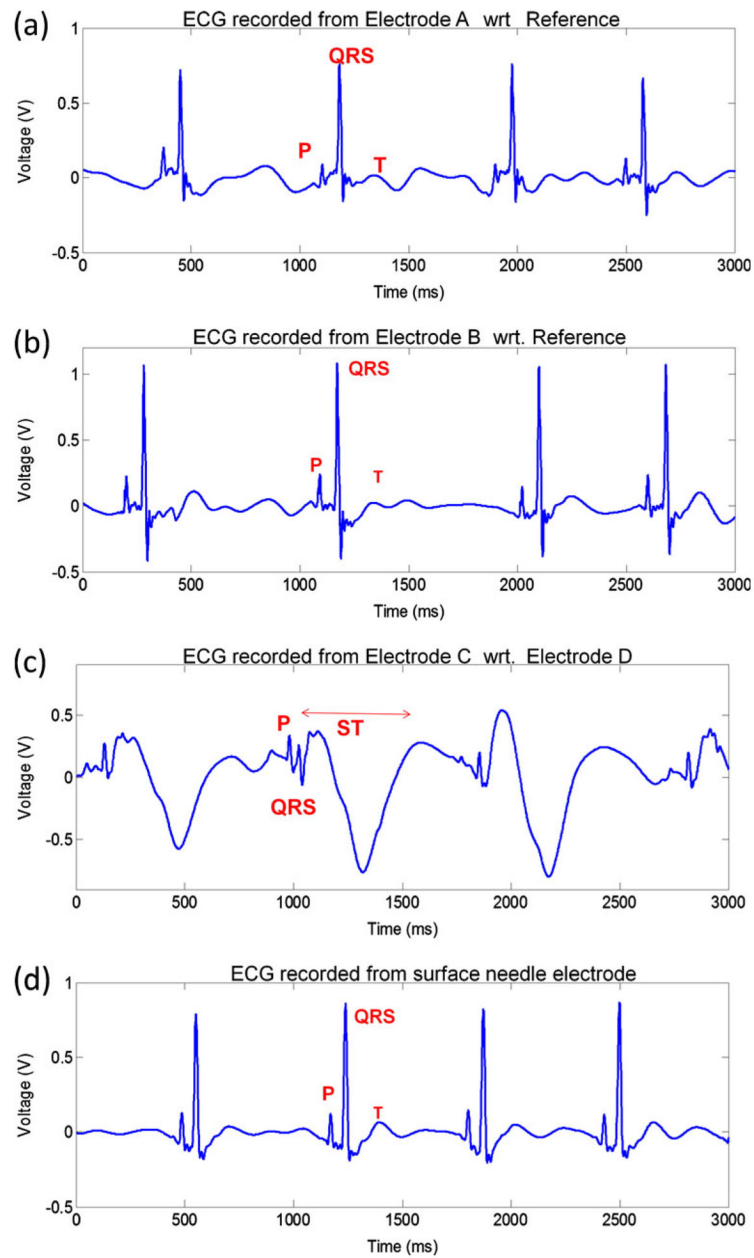


Fig. 4. (a) ECG signals recorded from Electrode A with respect to (wrt) the reference electrode. (b) Electrode B with respect to the reference. (c) Electrode C with respect to Electrode D. (d) ECG signals acquired by the use of surface needle microelectrodes. Signals after noise-reduction from epicardial microelectrode array demonstrated comparable signal strength (0.6–1.1 V vs. 0.8 V, respectively) as well as signal to noise ratio (7.1 dB vs. 7.4 dB, respectively) compared to surface needle ECG

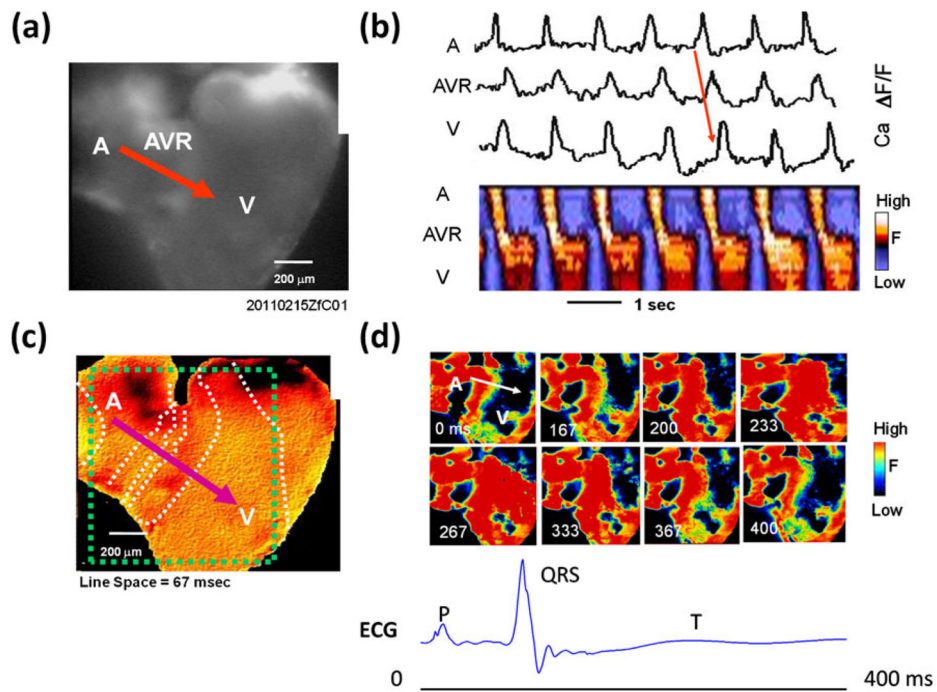
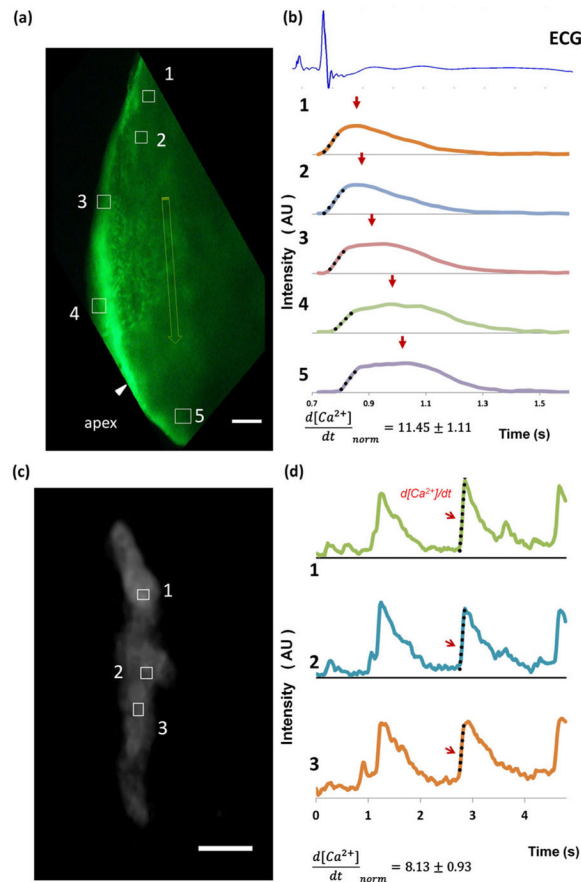


Fig. 5. Calcium transients in the entire zebrafish heart. **(a)** Raw optical Ca fluorescence image. A, atrium; AVR, AV ring; V, ventricle. Red arrow indicates the conduction direction. **(b)** Upper panel shows Ca_i transients traces from representative sites in the A, AVR and V. The lower panel shows line scans of Ca fluorescence along the red line in A, showing AV conduction velocity (slope of leading edge) is delayed through AVR compared to A and V. **(c)** Isochronal map showing the fast conduction velocity in both A (greater separation between dashed white isochrones) and slow conduction velocity through AV ring area (crowded isochrones). The dashed green square indicates the mapped area in panel D. **(d)** Pseudo-colored snapshots of Ca fluorescence at the various times indicated at the lower left of the each snapshot, *Red* = high calcium; *yellow* and *green* = intermediate calcium, and *blue-black* = low calcium. The white arrow shows the direction of conduction. Scale bars: 200 μm (**a**, **c**); 1 s (**b**)

**Fig. 6.**

(a) Apical region of a contracting ventricle was captured. Five ROIs were represented by boxes and the apex (edge not shown) was indicated by an arrow. Scale bar, 200 μm . (b) Corresponding mean fluorescence intensity plots of ROIs 1–5 revealed propagation of Calcium transients, normalized $d[Ca^{2+}]/dt$ of rising slope were calculated, $d[Ca^{2+}]/dt = 11.45 \pm 1.11$ ($n=5$), dotted lines represent linear fitting of slopes. From box 1 to box 5 that were superimposed in one epicardial ECG cycle (1.2 s). Arrows indicated peak amplitudes that were normalized to 1 with arbitrary unit (AU). (c) Three regions of interests (ROIs) denoted by white boxes 1, 2 and 3 were captured from a single contracting cardiomyocyte. Scale bar, 20 μm . (d) Corresponding mean grey value intensity plots of 3 ROIs illustrated Calcium transients. Second rising calcium transients were used to calculate normalized $d[Ca^{2+}]/dt$ ($d[Ca^{2+}]/dt = 8.13 \pm 0.93$, $n=3$) as indicated by arrows, dotted lines show linear fitting of three rising slope. Amplitude of calcium transients were normalized to 1, with arbitrary unit (AU)

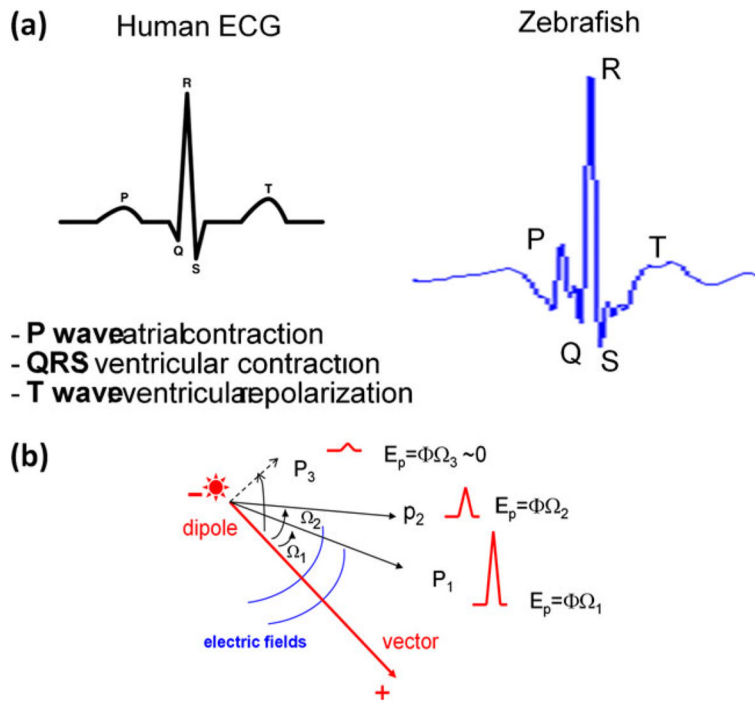


Fig. 7. (a) Comparison between human and zebrafish ECG signals. Due to a smaller heart size and higher mean heart rates, the PR interval for zebrafish is shorter than that of humans. T waves usually display a biphasic pattern acquired from the pseudo-unipolar electrodes. (b) Lead placements in relation to the vector direction. QRS amplitudes in P1 and P2 are dependent on the electrode lead position. E_p denotes electric potential, Ω the solid angle, and Φ the strength of charge surface ($\Phi = \text{voltage/unit of the solid angle}$)